ALGORITHM THEORETICAL BASIS DOCUMENT (ATBD): NEON ELEVATION (DTM AND DSM)

PREPARED BY	ORGANIZATION	DATE
Tristan Goulden	AOP	05/29/2019

APPROVALS	ORGANIZATION	APPROVAL DATE
David Barlow	SYS	06/11/2019

RELEASED BY	ORGANIZATION	RELEASE DATE
Anne Balsley	CM	07/01/2019

See configuration management system for approval history.

The National Ecological Observatory Network is a project solely funded by the National Science Foundation and managed under cooperative agreement by Battelle. Any opinions, findings, and conclusions or recommendations expressed in this material are those of the author(s) and do not necessarily reflect the views of the National Science Foundation.

Change Record

REVISION	DATE	ECO #	DESCRIPTION OF CHANGE
A	07/01/2019	ECO-06170	Initial Release

TABLE OF CONTENTS

LIST OF TABLES AND FIGURES

1 DESCRIPTION

1.1 Purpose

This document details the algorithms used for creating the NEON Level 3 Elevation (DTM and DSM) data product (NEON.DOM.SIT.DP3.30024), from Level 1 data, and ancillary data (such as calibration data), obtained via instrumental measurements made by the Light Detection and Ranging (LiDAR) sensor on the Airborne Observation Platform (AOP). It includes a detailed discussion of measurement theory and implementation, appropriate theoretical background, data product provenance, quality assurance and control methods used, approximations and/or assumptions made, and a detailed exposition of uncertainty resulting in a cumulative reported uncertainty for this product.

1.2 Scope

This document describes the theoretical background and entire algorithmic process for creating NEON.DOM.SITE.DP3.30024 from input data. It does not provide computational implementation details, except for cases where these stem directly from algorithmic choices explained here.

2 RELATED DOCUMENTS, ACRONYMS AND VARIABLE NOMENCLATURE

2.1 Applicable Documents

AD[01]	NEON.DOC.000001	NEON Observatory Design (NOD) Requirements
AD[02]	NEON.DOC.002652	NEON Level 1, Level 2 and Level 3 Data Products Catalog
AD[03]	NEON.DOC.005011	NEON Coordinate Systems Specification
AD[04]	NEON.DOC.001292	NEON L0-to-L1 discrete return lidar algorithm theoretical basis document
AD[05]	NEON.DOC.002293	NEON Discrete LiDAR datum reconciliation report
AD[06]	NEON.DOC.001984	AOP flight plan boundaries design
AD[07]	NEON.DOC.002890	NEON AOP Level 0 quality checks
AD[08]	NEON.DOC.001207	NEON imaging spectrometer geolocation algorithm theoretical basis document
AD[09]	NEON.DOC.001211	NEON AOP digital camera image orthorectification algorithm theoretical basis document
AD[10]	NEON.DOC.002649	NEON configured site list

2.2 Reference Documents

RD[01]	NEON.DOC.000008	NEON Acronym List
RD[02]	NEON.DOC.000243	NEON Glossary of Terms
RD[03]	NEON.DOC.001292	NEON elevation Algorithm (DTM and DSM) Theoretical Basis Document
RD[04]	NEON.DOC.001984	AOP flight plan boundaries design
RD[05]	NEON.DOC.005011	NEON Coordinate Systems Specification
RD[06]	NEON.DOC.001292	NEON L0-to-L1 discrete return lidar algorithm theoretical basis

2.3 Acronyms

Acronym	Explanation
DTM	Digital Terrain model
DSM	Digital Surface model
DEM	Digital Elevation Model
ITRF00	International Terrestrial Reference Frame 2000
UTM	Universal Transverse Mercator
TIFF	Tagged Image File Format
AOP	Airborne Observation Platform
FBO	Fixed Base Operator
PPM	pulses per square meter

3 DATA PRODUCT DESCRIPTION

3.1 Variables Reported

The elevation products supplied through NEON.DOM.SIT.DP2.30024 include a digital terrain model (DTM) and a digital surface model (DSM). The DTM shall include only elevations that relate to the physical terrain surface, while the DSM shall also include elevations that relate to surface features (eg. buildings, vegetation). Within this document the term DEM may also be used, which according to Maune (2007), is synonymous with DTM. For all references to NEON products, only DTM and DSM shall be used, while DEM is used in instances where the original terminology for an outside entity or author is preserved. For example, the USGS designates their elevation products as DEMs, therefore any mention of the USGS elevation product within this document will maintain their terminology. Elevations values for the NEON DTM and DSM are reported with reference to Geoid12A datum NGSGeoid12A, while horizontal coordinates are referenced to the ITRF00 datum, projected to the Universal Transverse Mercator (UTM) mapping frame in accordance with AD[03]. The DTM and DSM are separated into a set of 1 km by 1 km tiles, which have corners spatially referenced to an even kilometer. The product is stored in a GeoTIFF format in accordance with the GeoTIFF specification Ritter et al., (2000).

3.2 Input Dependencies

The creation of the DTM and DSM primarily requires LAS files. LAS files are an L1 product created from the L0 LiDAR data (see AD[04]). In addition to the LAS files, three additional sources of information are required

1. A raster image covering the continental U.S containing the vertical difference between the WGS84 and NAD83 ellipsoids in meters. This is used to vertically correct the elevation in the LAS files. Further details into the background of this correction can be found in AD[05]. The raster file was created in-house in GeoTIFF format, and is currently stored in SVN_AOP \DataProcessing\LidarProcessing\Lidar_ processing_ workflow_ external_ files\ITRF00_ 2_ NAD83_ coversion_ raster\ITRF00_ 2_ NAD83_ seperation.tif.
2. A USGS DEM which has larger spatial extent than the site boundary, used for identification of noise points. USGS DEMs are obtained from the National Map service provided by the USGS (http://nationalmap.gov/) in a 'Grid Float' format (binary file with FLT extension and associated header file). All USGS DEMs are currently stored in Z:\external\USGS_DEM in the appropriate domain and site folder.
3. A CSV file containing the four letter site code for all NEON sites and their associated domain, currently located in Z:\external\USGS_ DEM\site_lookup\site_lookup.csv.

3.3 Product Instances

The NEON data products produced directly from these algorithms are summarized in Table 1:

Table 1 - Data products generated by algorithms described within this ATBD

Data product identification	Data product name
NEON.DOM.SITE.DP3.30024	Elevation - Digital Terrain Model (DTM)
NEON.DOM.SITE.DP3.30024	Elevation - Digital Surface Model (DSM)

3.4 Temporal Resolution and Extent

The DTM and DSM product will include data collected during acquisition of a single core, re-locatable or aquatic site by the AOP. Depending on external variables such as weather, transit time to the site FBO, and total area of the priority 1 flight box (see AD[06]), the temporal resolution of a single acquisition of L0 LiDAR information used to produce the DTM / DSM could range from a single flight (4 hrs.) to several flights acquired over multiple days. Generally, due to the peak greenness constraint of AOP data acquisition (site at > 90% peak greenness value), and the requirement that all sites are to be flown annually, the total potential time to acquire a site will have a limit which defines the largest temporal resolution for a single acquisition. Details defining the total amount of potential time that could be dedicated to a single site acquisition, are given in AD[06]. As the NEON AOP payload is scheduled to repeat each NEON site on an annual basis, the temporal resolution of multiple acquisitions will be one year.

3.5 Spatial Resolution and Extent

The DTM and DSM shall be interpolated to a raster format with a 1 m spatial resolution. LiDAR acquisitions by the NEON AOP are designed to nominally produce 3-4 ppm (pulses per m2), however due to acquisition constraints at some sites the ppm will be lower. To confidently allow creation of the DTM and DSM at a 1 m spatial resolution, NEON AOP LiDAR acquisitions will be designed to collect a minimum of 1 ppm. The choice of 1 m spatial resolution is also selected to match the spatial resolution of the NIS (NEON Imaging Spectrometer), which is co-mounted with the LiDAR sensor in the AOP. The planned spatial extent of the DSM and DTM will relate to the definition of the AOP flight box for each individual site (AD[06]). It is intended that a minimum of 80% of the priority 1 flight box and 95% of the tower airshed will be acquired each year (AD[07]). As discussed in Section 3.4, the actual acquisition area could vary depending on external conditions encountered during the flight. Ultimately, the flight schedule as defined in AD[06] will supersede the percent coverage requirement. Therefore, the actual acquired spatial extent may vary annually.

4 SCIENTIFIC CONTEXT

The elevation product, in the form of a DTM provides information on terrain structure, which influences the governing hydrological processes (flow and erosion) occurring within a landscape. Hydrological processes

impact the spatial distribution of flora and fauna (Moore et al., 1993), and the resultant site ecology. Therefore, the DTM is an important data layer in spatially driven models of landscape processes, and these models allow for spatially explicit predictability of phenomena internal and external to the landscape. Currently, LIDAR sensors provide the most efficient means for collecting an accurate and dense sample of the terrain among competing remote sensing or positioning systems. For example, high-resolution digital stereo photogrammetry can compete in terms of point density in open terrain, but suffers from sparse sampling beneath tree canopy.

The DSM provides two important functions as complimentary information to the optical sensors on the AOP (imaging spectrometer and high resolution RGB camera). The first function is strictly as a tool in the geolocation processing of the hyperspectral sensor and the RGB digital camera (see AD[08] and AD[09] respectively). During geolocation, the LiDAR derived DSM provides a surface used in ray-tracing the direction of acquisition of individual pixels acquired by the spectrometer and digital camera. The high accuracy and spatial resolution of the LiDAR derived DSM provide enhanced accuracy to the geolocation process. The DSM also provides information on the structure of surface features. Of particular importance at NEON is LIDAR derived vegetation structure, which can be used as a proxy to estimate important ecological quantities of interest across the differing eco-climatic domains. The vegetation structure information can be combined with the spectrometer measurements to provide enhanced information for identification and classification of vegetation at the species level Anderson et al, (2008), Asner et al., (2007), Paris and Bruzzone (2015).

4.1 Theory of Measurement

Airborne LiDAR systems capture information of the earth's topography as a set of discrete three-dimensional coordinate observations, commonly referred to as a 'point cloud.' Although it is possible to extract information directly from the point cloud, it is more common to covert the discrete data points to a continuous surface. The most common form of a continuous elevation surface is a grid-based representation (Moore et al., 1993; Fisher et al., 2006), also known as an elevation raster. The elevation raster contains a set of regularly spaced points in a horizontal plane, and each point has an associated elevation above a given datum. The grid based structure is attractive because it forms a simple topological relationship between elevation values and allows computational efficiency when processing to downstream products. The discrete points as-captured by the LiDAR will not be in the desired grid structure, but will be distributed in a pseudo-random pattern across the landscape (**Figure 1**) which is dependent on acquisition parameters. To determine the elevation at the pre-determined horizontal grid cell locations, an interpolation routine must be employed to estimate the elevation between discrete points. An elevation raster interpolated from LiDAR points derived from reflections occurring from the ground surface is termed a DTM (Digital Terrain Model). An elevation raster containing points reflected from surface features such as buildings and vegetation, as well as ground points, is termed a DSM (Digital Surface Model).

4.2 Theory of Algorithm

4.2.1 Interpolation Routine

A Delaunay triangulation is used to generate a triangular irregular network (TIN) from the discrete LiDAR points to provide a continuous surface from the discrete LiDAR points and facilitate interpolation to a raster (**Figure 1**, **Figure 2**). The Delaunay triangulation constructs a series of contiguous triangular facets that form linear connections between adjacent points in the point cloud. The Delaunay triangulation is constrained in that no point is within the circumcircle of any other triangle, and the minimum angle in any given triangle is maximized De Berg et al., (1997). A raster grid with evenly spaced cells that covers the TIN is created, and the elevation is extracted from the triangular plane at the horizontal location of each grid point (**Figure 2**). The grid cells are created with a 1 m spacing which provides the 1 m spatial resolution discussed in Section 3.5.

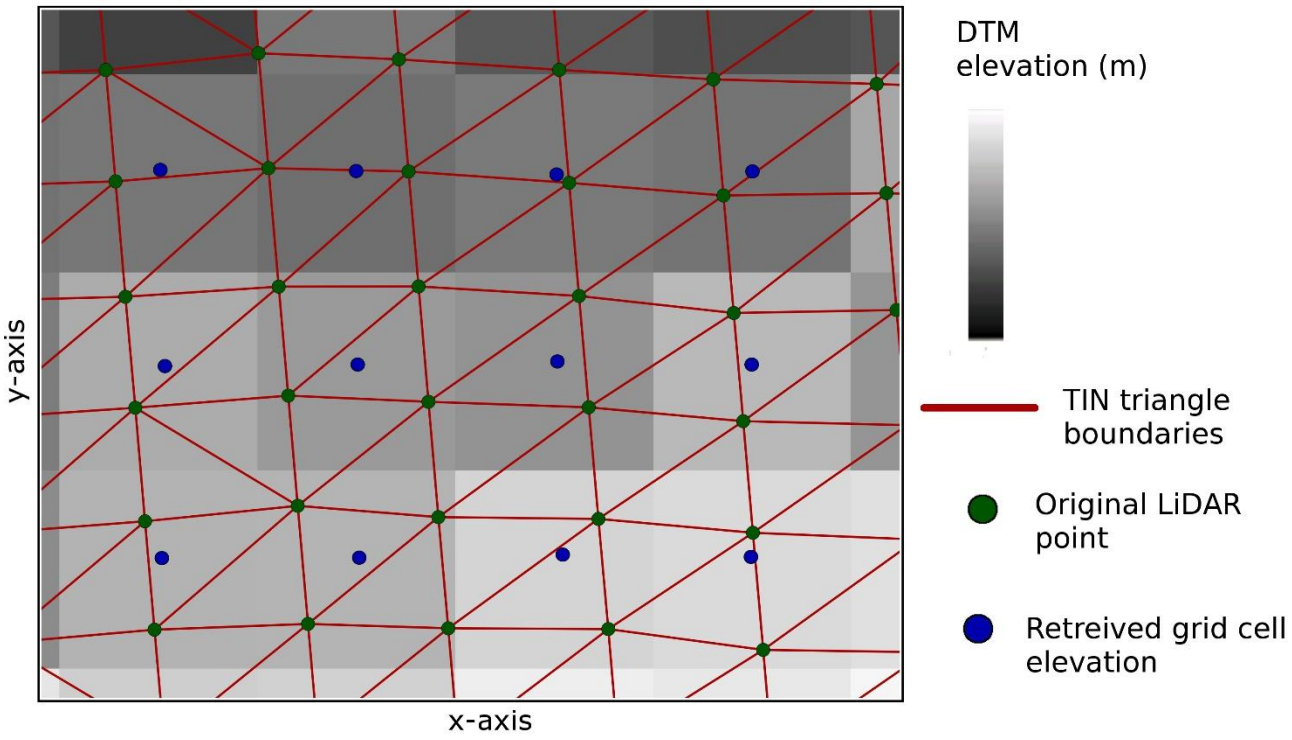

Figure 1 - Example distribution of discrete LiDAR points and grid cell locations

4.2.2 Pre-processing

Prior to creation of the DSM and DTM, the LAS files are analyzed to identify returns within the point cloud that can be considered outliers. Outliers can occur as a result of various atmospheric and terrain conditions. For example, particulate matter in the atmosphere that lies in the optical path of the laser pulse can reflect sufficient photons to register a return signal and will result in undesirable points well

above the terrain. Returned signal which has experienced multiple reflections that deflect the pulse away from the projected beam centerline can result in erroneously long ranges and cause points to exist below the terrain. The existence of outliers will result in artifacts in the DSM and DTM and must be flagged as noise during pre-processing. According to the ASPRS (American Society of Photogrammetry and Remote Sensing) LAS 1.3 specification, noise points are given the classification integer '7'. This convention is maintained. Following USGS recommendations, the outlying points will still exist within the LAS files, but are ignored during DTM and DSM processing (Heidemann, 2014). Noise points are identified through two methods:

1. identifying isolated points,
2. identifying points outside of elevation threshold surrounding a USGS DEM.

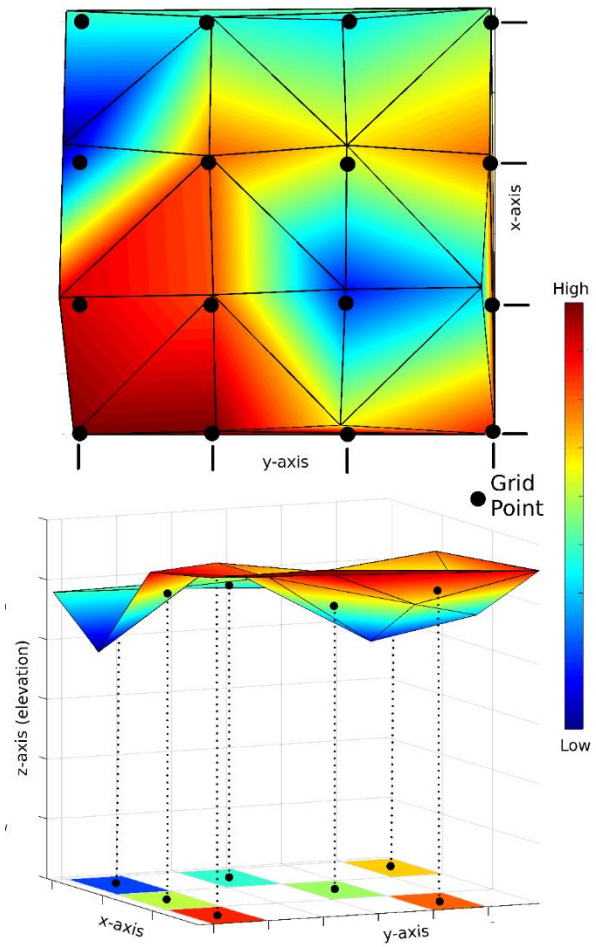

Figure 2 - Sample of points interpolated from the elevation of a TIN surface to a raster grid

Identification of isolated points (method 1) is performed by specifying a volume in which a maximum number of points can be located. For example, if a maximum of *X* points is found within a volume of *Y* m^3, all points will be flagged as noise, where the current default selections of *X* and *Y* is four and five respectively. This noise identification routine is ideal at locating single atmospheric hits or undesirable objects on the terrain such as utility poles. In method 2, a USGS DEM is used to flag noise points by identifying elevation thresholds above and below the DEM. Points outside the threshold are considered outliers and flagged as noise. The USGS DEM is obtained from the National Map (details in Section 3.2). Currently thresholds are set at 50 m above the terrain and 25 m below the terrain. These noise identification routines will locate larger groups of outlying points which may have been too numerous to be identified in method 1.

After noise identification, the point cloud is separated into a series 1 km by 1 km tiles with an associated buffer, currently set at 25 m. The data are divided into tiles to allow the TIN algorithm to operate without computer memory constraints. Testing has revealed that under nominal flight acquisition parameters, the 1 km by 1 km tile size is sufficiently small to avoid memory issues. However, if special engineering flights are conducted which result in point densities higher than nominal acquisition parameters, the tile size will have to be reduced. The buffer associated with each tile is designed to eliminate edge artifacts at tile boundaries. The DTM / DSM tiled product will have the buffer removed.

Following tiling, the point cloud is classified into ground and non-ground points (**Figure 3**). The ground point filtering algorithm implements a variation of the Axelsson (2000) TIN refinement algorithm. The filtering algorithm requires several input parameters that can be modified based on the structure of the terrain. End- member cases of parameter selection include urban areas containing buildings with long (> 25 m) edges and natural landscapes without abrupt changes in elevation (cliffs). As most of the NEON

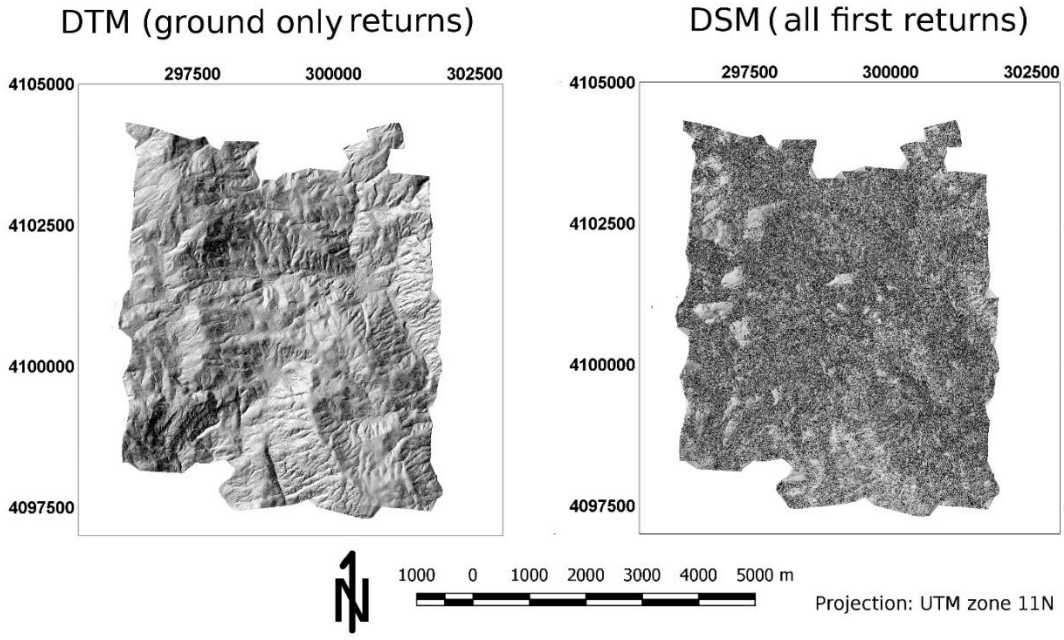

Figure 3 - Left: Hill-shade representation of the DTM of NEON SOAP site (ground points), Right: Hill-shade representation of the DSM of NEON SOAP site (all first returns)

sites consist of the latter, parameters have been optimized for this type of landscape. As a result, anthropogenic modifications to the landscape, abrupt changes in elevation (cliffs), or discontinuous surfaces have resulted in a decrease in performance of the filtering algorithm. In these circumstances, some unwanted surface features may be visible in the DTM (discussed further in Section 6.1).

Once the data has been separated into 'ground' and 'non-ground' classes, the 'non-ground' class is further sub- divided into 'building', 'high-vegetation' and 'unclassified' classes. Testing has revealed that ideal natural landscape conditions can produce a large number of points classified as 'unclassified'. The 'unclassified' class represents points that the classification algorithm determined were ambiguous. Ideally, the DSM could be created from only the ground, building and vegetation classes, leaving the 'unclassified' points ignored. However, analysis of the 'unclassified' points revealed that a significant number of returns from vegetation features were generally included in the 'unclassified' class and their inclusion improved the accuracy of the DSM. Therefore, points classified as 'unclassified' are included in DSM creation.

4.2.3 Post-processing

A consequence of including the 'unclassified' points is that points erroneously located below the ground, but within the noise identification threshold (see Section 4.2.2), will be included in DSM creation. This causes some DSM cells to exist at a lower elevation than the equivalent cell in the DTM. This will introduce artifacts into higher-level data products, such as negative values in canopy height models (determined as a subtraction of the DTM from the DSM). To correct the issue, the DSM and DTM are compared and any cell in the DSM that is lower than the DTM is raised to the height of the DTM. This process is represented by the dotted line in Error! Reference source not found..

4.3 Special Considerations

One of the advantages of a TIN interpolation routine is that it honors the locations of the observed data points and makes minimal assumptions about the structure of the terrain (as linear connections along triangular edges are used). However, NEON AOP LiDAR acquisitions will result in a maximum spacing between points that is often less than the grid cell size (spatial resolution) and results in several LiDAR points within each raster grid cell. Each LiDAR point position is influenced by random errors, which have shown dependence on acquisition parameters (Glennie, 2007; Goulden and Hopkinson 2010) and terrain conditions Schaer et al., (2007), Goulden and Hopkinson (2014) and vegetation (Hopkinson et al., 2005; Reutebuch et al., 2003). The TIN algorithm does not exploit the available redundancy in the LiDAR observations to reduce the influence of random error through averaging. As a result, the DTM / DSM can appear noisy and the random error can propagate to downstream data products. To reduce the influence of random errors, it is recommended that a 3 x 3 moving average boxcar filter is applied to the DTM prior to creation of downstream products. However, the DTM and DSM product, as delivered, have not been modified in this fashion in order to preserve their original fidelity.

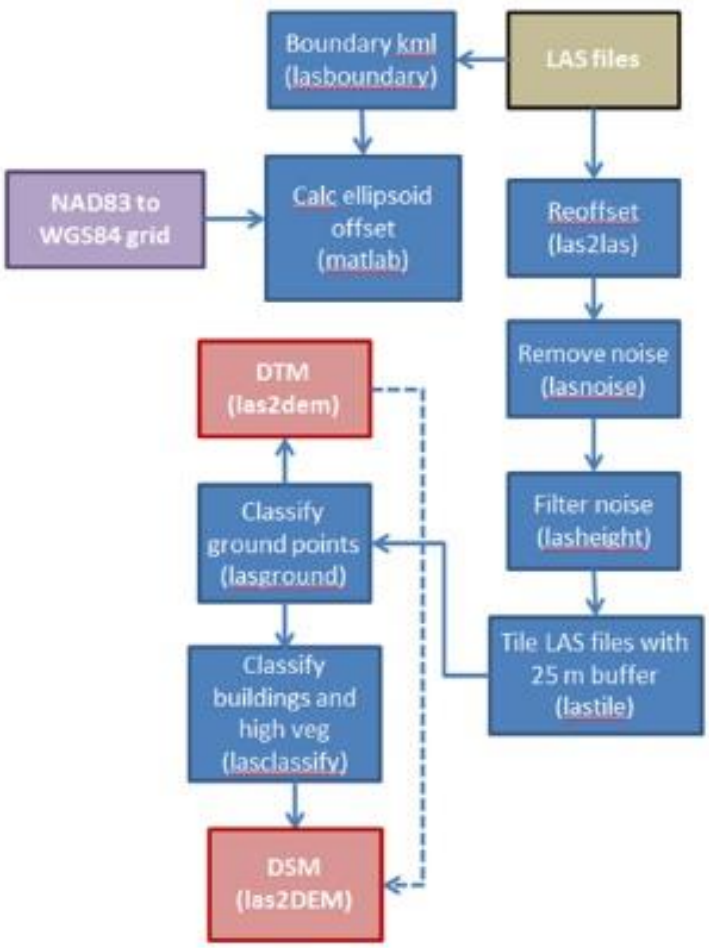

Figure 4 - Flowchart for creation of the DTM and DSM

5 ALGORITHM IMPLEMENTATION

The processing of the LAS files to the DTM / DSM products is achieved through the following steps (Error! R eference source not found.). The steps are connected through a SHELL script that shall be implemented through a Cygwin terminal (https://www.cygwin. com/) that allows automation of the algorithm. Cygwin is required because the SHELL script calls functions from the LAStools software package, which consists of a collection of windows executables. Cygwin allows the windows exe- cutables to be run in an environment similar to LINUX / UNIX, but without requiring the lastools executables to be in a LINUX compatible format.

Step 1:

Create a KML file describing the boundary of the flight from all LAS files obtained during the flight.

Input: all LAS files

Output: KML file of entire flight boundary named full_boundary.kml

Functions used: lasboundary.exe

Step 2:

Determine the corrective vertical translation to correct for the separation between NAD83 and ITRF00 ellipsoids. The location to retrieve the corrective factor is obtained from the averaged extents of the flight box obtained in step 1.

Input:

1. KML boundary from step 1 (full_boundary.kml),
2. Geotiff file containing the vertical translations between ITRF00 and NAD83 (see Section 3.2).

Output: Text file containing the vertical correction (conversion.txt)

Functions used: read_kml_from_lasboundary.m, calc_ellipsoid_translation_lastools_v2.m

Step 3:

Apply the corrective factor determined in Step 2 to the LAS files.

Input:

1. LAS files,
2. Conversion.txt from step 2

Output: LAS files with '_reoffset' suffix added to the file name prior to LAS file extension

Functions used: las2las

Step 4:

Identify isolated noise points from the LAS files. A maximum number of points which are isolated within a predefined volume are flagged as noise. The volume and number of points are set with 'step_ size' and 'isolated' flags.

Input:

1. LAS files with '_reoffset' suffix from step 3,
2. Step size and isolated flags (currently set to 4 and 5 respectively).

Output: LAS files with a '_denoise' suffix added to the file name prior to LAS file extension

Functions used: lasnoise

Step 5:

Convert a USGS from its native FLT format to ASCII format

Input:

1. Site to domain lookup csv file (see Section 3.2),
2. Site boundary kml (from step 1),
3. Four letter site code,
4. UTM zone number

Output: DEM ASCII file of USGS cell coordinates and elevations with name SITE_ USGS_ DEM.csv, where SITE is the four letter code of the NEON designated site (see AD[10])

Functions used: create_ascii_file_from_FLT_lastools.m

Step 6:

Convert the ASCII file created in Step 5 to a LAS file.

Input: SITE_USGS_DEM.csv from step 5.

Output: LAS file with name SITE_USGS_DEM.las

Functions used: txt2las

Step 7:

Filter the input LAS files based on the USGS DEM LAS file. This step will identify any points that fall outside of a defined buffer above and below the USGS DEMs and flag them as noise. Current buffers set as 100 m above the USGS DEM and 25 m below the USGS DEM.

Input:

1. LAS file containing USGS DEM information created in step 6 (SITE_USGS_DEM.las),
2. Above and below ground buffer flags (100 and 25 respectively)

Output: LAS files with additional noise points flagged with '_filtered' added as a suffix to the filename before the file extension.

Functions used: lasheight

Step 8:

Tile the LAS data with '_ filtered' extension into 1 km by 1 km tiles with a buffer of 25 m.

Input:

1. Filtered LAS data from step 7,
2. Buffer value flag (25),
3. Tile size flag (1000)

Output: Tiled LAS files.

Functions used: lastile

Step 9:

Classify the LAS data into ground and non-ground points.

Input:

1. Tiled LAS data from step 8,
2. Flag which identifies the search mode,
3. Flag which indicates the size of a search area for identification of original ground points,
4. Offset flag.

Output: Tiled LAS files with ground points classified according to ASPRS classification scheme LAS13Spec.

Functions used: lasground

Step 10:

Create a DTM from each ground filtered tile using the TIN algorithm.

Input:

1. Ground classified tiled LAS data from step 9,
2. Step size flag to indicate spatial resolution (1 m),
3. Elevation flag to indicate elevation is the variable used to create the TIN,

4. Kill triangles flag to indicate the maximum size of a triangular edge to be maintained (250 m),
5. Keep class flag to indicate which point classifications to use (i.e. only ground points here).

Output: Grid based DTMs at 1 meter spatial resolution in geotiff format with a 'YYYY_ SITE_ V01_ DTM' filename before the file extension, where YYYY is the year the data was acquired, and V01 indicates the version number.

Functions used: las2dem

Step 11:

Classify points into buildings, high vegetation, and unclassified.

Input:

1. Ground classified tiled LAS data from step 9,
2. Planer flag to indicate expected standard deviation of points to aid in identifying planer features.

Output: Tiled LAS files with ground, building, vegetation, and unclassified points classified according to ASPRS classification scheme LAS13Spec.

Functions used: lasclassify

Step 12:

Create a DSM from each tile using the TIN algorithm.

Input:

1. Classified tiled LAS data from step 11,
2. Step size flag to indicate spatial resolution (1 m),
3. Elevation flag to indicate elevation is the variable used to create the TIN,
4. Kill triangles flag to indicate the maximum size of a triangular edge to be kept (250 m),
5. Keep class flag to indicate which point classifications to use (i.e. only ground points, building, vegetation and unclassified here)

Output: Grid based DSMs at 1 meter spatial resolution in geotiff format with a 'YYYY_ SITE_ V01_ DSM' filename before the file extension

Functions used: lasclassify

Step 13:

Quality check ensuring all DTM grid cells are lower than DSM cells (represented by dashed line in Error! R eference source not found.**)**

Input: Geotiff tiles from step 10 and step 12.

Output: Modified DSM tiles in geotiff format.

Functions used: combine_ DTM_ DSM_ gtif_ LASTOOLS.m

6 UNCERTAINTY

6.1 Analysis of Uncertainty

Fisher and Tate (2006) separates sources of uncertainty in DEMs into three broad categories:

1. errors related to the sensor or instrument used to acquire the data.
2. errors related to the processing and interpolation of the data.
3. errors introduced by the structure of the terrain / landscape

An analysis of uncertainty in LiDAR DTM / DSMs through category (1) can be obtained by propagating the errors of the LiDAR sensor sub-systems to each point in the point cloud and then through to each individual raster cell of the DTM / DSM. Background information into the algorithmic details of propagation of system component errors into each individual point in the point cloud is described in AD[04], adapted from the algorithm given in Goulden and Hopkinson (2010). Currently, an algorithm to further propagate system component errors into the DTM / DSM has not been implemented. An example scenario which does propagate system component errors into LiDAR derived DTMs can be found in Goulden and Hopkinson (2014), demonstrating it is a theoretically and practically viable option.

Propagating errors from the sensor sub-systems (category 1) alone ignores the uncertainty introduced through category (2) and category (3). Within category (2), uncertainty in LiDAR derived DTM / DSMs is introduced through two processing components a) interpolation, and b) classification errors of the point cloud. Several studies have attempted to quantify the uncertainty due to interpolation on LiDAR derived DTM / DSMs. For example, Hodgson and Bresnahan (2004) found that interpolation errors were of lower magnitude than system related errors, and Bater and Coops (2009) found that interpolation errors were generally sub-centimeter, indicating that interpolation error may be negligible. However, these statements should be qualified with landscape conditions and point density. Interpolation error will tend to be higher in landscapes with highly variable or sloped terrain Su and Bork (2006) or in instances where point spacing can be low Lloyd and Atkinson (2002), such as ground points under dense forest canopy. Generally, due to the dense sampling provided by the nominal collection rates of the NEON LiDAR sensor, uncertainty due to interpolation is likely to be minor. Therefore, uncertainty introduced through interpolation will not be explicitly quantified and reported.

Qualitative analysis of LiDAR data acquired by the NEON AOP has revealed that misclassification errors (category 2, processing component ‘b’) are generally present. For example, steep cliff edges are often classified as non-ground points because of the ambiguity between the rapid change associated with building edges and cliff features (**Error! Reference source not found.**). Commonly observed errors in m isclassification also occur when building rooftops are classified as ground, and when vegetation is classified as ground. A human analyst can often qualitatively identify these types of errors; however, they pose problems for quantitative analysis. Unfortunately, the uncertainty introduced through point misclassification (as shown in the example of steep cliff edges in **Error! Reference source not found.**) can r

esult in the largest sources of uncertainty in the final DTM / DSM. Due to the difficulty in obtaining sufficient ground truth data to identify misclassifications, the uncertainty due to this component will not be strictly quantified. However, users should be aware of its existence.

Uncertainty due to category 3 is less straightforward to define, as the introduced uncertainty is fundamentally linked to the representation of a continuous phenomenon (terrain) through discrete data. The spatial resolution defines the sampling frequency of the discrete signal used to represent the continuous terrain, and can have profound consequences to the development of downstream data products. A simple example is terrain slope, which tends to decrease on average as the spatial resolution decreases (Chang and Tsai, 1991, Kienzle, 2004; Hopkinson et al., 2010) and finer details of the topography cannot be represented. Generally, the higher resolution the DTM / DSM, the more representative it will be of the true terrain shape. Although this infers that high resolution DTM / DSMs are superior, implementing the DTM / DSM into spatially driven models which were not designed or tested to ingest fine scale terrain models may lead to a high level of uncertainty in model outputs. For example, systematic relationships have been generally observed in various hydrological models, which commonly implement DTMs as an input data layer. Quinn et al. (1991) and Zhang and Montgomery (1994) identified that peak flow rates will decrease as DTM resolution increases, and Thieken et al. (1999) scaling noted peak flow timing will be delayed. In a small agricultural watershed, Goulden et al., (2014), showed that the SWAT hydrological model will only simulate sediment loads adequately with 1 m resolution DTMs if the model parameterization is deviated from realistic values. Although the uncertainty resulting from category 3 is not directly measureable, these analyses show that users of NEON supplied DTMs should exercise due diligence when implementing the DTM / DSM for their particular application.

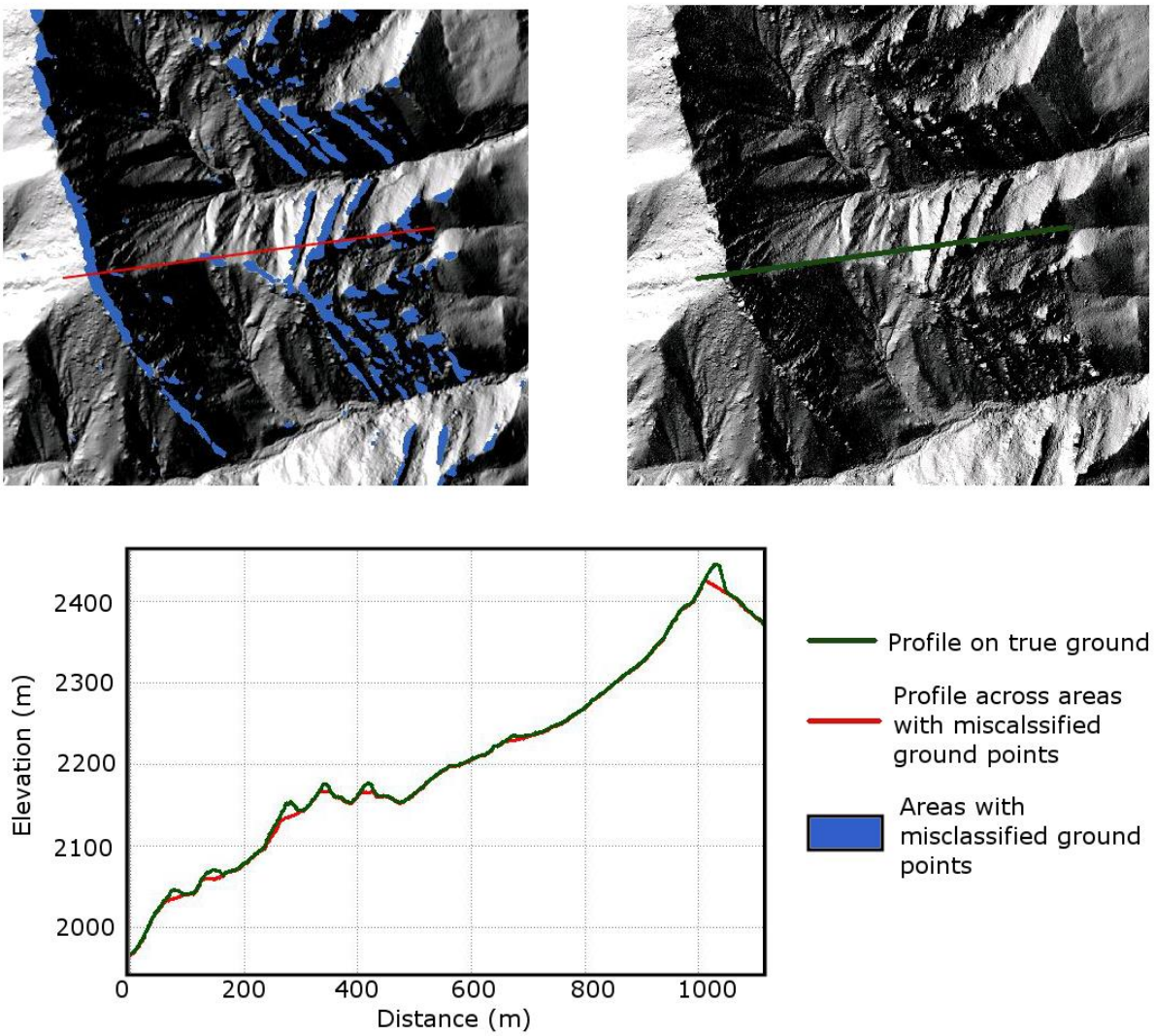

Figure 5 - Flowchart for creation of the DTM and DSM

6.2 Reported Uncertainty

Currently, no uncertainty is reported with the DTM / DSM product. In the future, the vertical uncertainty associated with each grid cell will be reported in a separate raster of uncertainty values. The uncertainty will be obtained from the system errors propagated through to the point cloud, as discussed in AD[04], and then propagated further into the DTM / DSM. It should be noted that this form of communicating uncertainty in DTMs / DSMs defies current convention that typically provides a single RMSE value for reporting error in a DTM. Although common, this form of reporting uncertainty has faced criticism for not describing the spatial pattern of uncertainty within the DTM Wechsler (2007), Fisher et al. (2006), and for not providing information on the various sources of contributing error (Hunter and Goodchild, 1996).

Wechsler (2007) notes that the primary historical reason for use of a single RMSE value is due to end-users not allocating sufficient financial resources to contract service providers to produce spatially explicit maps of uncertainty, and that end-users typically do not have access to the necessary information on error sources to propagate errors into the DTM themselves. Wechsler (2007) notes that DTM vendors have been encouraged to provide spatially explicit maps of uncertainty (see Kyriakidis et al., 1999), although this has not yet become general practice. As NEON has access to the raw data used to produce the DTM, it provides an opportunity to follow the recommendation made by Wechsler (2007), and provide spatially explicit rasters of DTM / DSM uncertainty propagated from system errors.

7 VALIDATION AND VERIFICATION

7.1 Algorithm Validation

As the majority of the algorithm is implemented with the LAStools commercial software package, there is limited validation that can be performed on these components. However, the LAS file inputs can be validated prior to algorithm execution with LASvalidate. LASvalidate is part of the LAStools distribution, and ensures each input LAS file is compliant with the ASPRS specification (ASPRS, 2013). Noncompliance will result in a warning or failure by LASvalidate. Outputs of the algorithm are visually inspected to ensure that 1) an appropriate number of files have been created and 2) the values in the outputs are reasonable. For example, the DTM can be compared with a USGS DEM to ensure the results are comparable within their respective error tolerances. If sites have been previously flown by the AOP a DTM subtraction will be performed against the previously created DTM and analyzed for differences outside of the error tolerances of the DTM acquisitions. A similar differencing operation cannot be performed with the DSM because of the dynamic nature of vegetation that is expected to change between acquisitions.

7.2 Vertical validation and verification

The ASPRS developed the document “New standard for new era: Overview of the 2015 ASPRS positional accuracy standards for digital geospatial data”, which details standards and methodology for validating the quality of geospatial data, including LiDAR-derived DTMs (see Abdullah et al., 2015). Since their release, the standards have been adopted by the United States Geological Survey (Heidemann, 2014) as methodology for reporting uncertainty for LiDAR products delivered to USGS. According to Abdullah et al., (2015), validation of the vertical component (elevation) of the DTM is assessed by comparing DTMs against checkpoints. Checkpoints are three-dimensional coordinates obtained from a source of higher accuracy, such as static GPS observations. The checkpoint elevation is compared against an interpolated elevation from the DTM at the same horizontal location as the check-point. Several checkpoints must be observed to develop a robust statistical sample to provide reliable statistical metrics (see Section 6.2). Methodology for collecting check points can be found in Abdullah et al (2015).

The validation of the vertical component is separated into non-vegetated vertical accuracy (NVA) and a vegetated vertical accuracy (VVA)(Abdullah et al., 2015). Vegetated and non-vegetated areas are

separated because it is assumed that errors in non-vegetated area will be normally distributed, and errors in non-vegetated areas will not be normally distributed. The metric for quantifying the uncertainty is the 95% confidence interval in the non-vegetated case (standard deviation of errors *1.96), and the 95th percentile of errors in the vegetated case. The validation results separate the DTM into discrete classes of quality levels. For example, the 5 cm vertical accuracy class is associated with a 9.8 cm (5 cm *1.96) RMSE in non-vegetated classes, and 15 cm (5 cm*3) 95th percentile in vegetated areas. Note that the RMSE is interchangeable with the standard deviation for the assessment in non-vegetated areas because it is assumed that any mean bias is negligible (Abdullah et al., (2015). Verification by this means will only be performed at NEON sites where appropriate checkpoints are available.

7.3 Horizontal validation and verification

Abdullah et al., (2015) provide the following formula for verifying the horizontal uncertainty in LiDAR observations:

$$\in_{xy_{Total}} = \left(\in_{xy_{GNSS}}\right)^2 + \left(\frac{tan \in_{IMU}}{0.55894170} H\right) \quad (1)$$

where $\in_{xy_{Total}}$ is the total horizontal error, $\in_{xy_{GNSS}}$ is the horizontal error introduced by the GNSS positioning system, ϵIMU is the error introduced by the IMU (inertial measurement unit) and H is the above ground altitude. Although this formula facilitates an easily quantified value of horizontal uncertainty, it does not necessarily account for all factors contributing to the horizontal uncertainty such as beam divergence, and the influence of scan angle and aircraft attitude on horizontal uncertainty. These factors have shown to be important in quantifying the horizontal uncertainty in the point cloud (Goulden and Hopkinson, 2010). Therefore, implementation of Equation (1) will be an optimistic estimate of the overall horizontal uncertainty, especially given that the Optech Gemini sensor aboard the AOP is nominally operated in wide beam divergence and Equation (1) does not consider the beam divergence. For example, if we can assume a horizontal error of 0.05 m in x and y from the GNSS ($\in_{xy_{GNSS}}$ = 0.05), and an $\in_{IMU}$ error of 0.008° Applanix (2012), and H of 1000 m, the resulting horizontal error is 0.25 m. The wide beam divergence setting on the Optech Gemini is 0.8 mRad Ussyshkin and Smith (2006), which leads to a horizontal error of 0.4 m (0.8/2 *1000) from the beam divergence component alone. Therefore, use of Equation (1) for verifying horizontal uncertainty in the DTM / DSM is not realistic for a LiDAR sensor as operated by NEON. Although Abdullah et al (2015) do not provide an explanation to the use of the constant of 0.55894170 in the denominator of the fraction in Equation (1), modifying this value to 0.15 will provide a better estimation of the horizontal error at the nominal AOP flight altitude of 1000 m, which is approximately 0.58 m. This can be written as:

$$\in_{xy_{Total}} = \left(\in_{xy_{GNSS}}\right)^2 + \left(\frac{tan \in_{IMU}}{0.15} H\right) \quad (2)$$

without knowledge of the original derivation of the constant, it is unknown whether the relationship in Equation (2) will be valid at alternative values of H.

Alternatively, an empirical assessment of horizontal uncertainty can be achieved by collecting checkpoints similar to the assessment of vertical uncertainty. To perform a horizontal verification, checkpoints must be collected along the edge of break-lines in the terrain, such as building edges. The location of the break in the point cloud can then be compared against the break-line defined by the checkpoints. Although this provides validation of the error in the point cloud, it can be used as a proxy for the resultant error in the DTM / DSM. This type of verification will not typically be employed for each NEON site, however, will be performed upon the commissioning of each LiDAR sensor for acceptance into the AOP. It will be assumed that the results obtained from the commissioning test can be extrapolated to the data collected at each site. The analysis may be repeated periodically throughout the lifetime of the sensor.

8 FUTURE PLANS AND MODIFICATIONS

The most critical future modification to the algorithm will include modifications to the filtering and classification routines, the method of DTM interpolation, and the addition of uncertainty rasters (see Section 6.2). Currently, the filtering and classification of LiDAR points is a subject of on-going research and investigation. The Axelsson (2000) algorithm has become an industry standard algorithm as it is also used in the popular TerraScan (Terrasolid, Finland, http://www.terrasolid.com/home.php) suite software package. New developments to filtering and classification are on-going and as improvements to these algorithms are accepted by the community they will be incorporated into the algorithm. The TIN interpolation algorithm, although efficient and functional, may not be the most accurate interpolation routine. As mentioned in Section 4.3, the TIN algorithm does not exploit the redundancy in the LiDAR observations to effectively reduce the inherent noise in individual point observations. Further testing on common alternative interpolation routines such as IDW, nearest neighbor, natural neighbor, splines, and kriging can be tested and adopted if proven to provide a higher fidelity DTM / DSM.

9 BIBLIOGRAPHY

Abdullah, Q., Maune, D., Smith, D., & Heidemann, H. K. (2015). New standard for new era: Overview of the 2015 ASPRS positional accuracy standards for digital geospatial data. *Photogrammetric Engineering & Remote Sensing*, *81*(3), 173-176.

Applanix, (2012). POS AV 510 Specification, URL: https://www.applanix.com/pdf/specs/postrack_oem_specs.pdf. Last accessed: 2019-05-29

Anderson, J. E., Plourde, L. C., Martin, M. E., Braswell, B. H., Smith, M. L., Dubayah, R. O., ... & Blair, J. B. (2008). Integrating waveform lidar with hyperspectral imagery for inventory of a northern temperate forest. *Remote Sensing of Environment*, *112*(4), 1856-1870.

Asner, G. P., Knapp, D. E., Kennedy-Bowdoin, T., Jones, M. O., Martin, R. E., Boardman, J. W., & Field, C. B. (2007). Carnegie airborne observatory: in-flight fusion of hyperspectral imaging and waveform light detection and ranging for three-dimensional studies of ecosystems. *Journal of Applied Remote Sensing*, *1*(1), 013536.

ASPRS. (2009). Las specification, version 1.3–r10. The American Society for Photogrammetry & Remote Sensing (ASPRS).

Axelsson, P. (2000). DEM generation from laser scanner data using adaptive TIN models. *International archives of photogrammetry and remote sensing*, *33*(4), 110-117.

Bater, C. W., & Coops, N. C. (2009). Evaluating error associated with lidar-derived DEM interpolation. *Computers & Geosciences*, *35*(2), 289-300.

Chang, K. T., & Tsai, B. W. (1991). The effect of DEM resolution on slope and aspect mapping. *Cartography and geographic information systems*, *18*(1), 69-77.

De Berg, M., Van Kreveld, M., Overmars, M., & Schwarzkopf, O. (1997). Computational geometry. In *Computational geometry* (pp. 1-17). Springer, Berlin, Heidelberg.

Fisher, P. F., & Tate, N. J. (2006). Causes and consequences of error in digital elevation models. *Progress in physical Geography*, *30*(4), 467-489.

Glennie, C. (2007). Rigorous 3D error analysis of kinematic scanning LIDAR systems. *Journal of Applied Geodesy jag*, *1*(3), 147-157.

Goulden, T. & Hopkinson, C. (2010). The forward propagation of integrated system component errors within airborne lidar data. Photogrammetric Engineering & Remote Sensing, 76(5), 589–601.

Goulden, T., & Hopkinson, C. (2014). Mapping simulated error due to terrain slope in airborne lidar observations. *International journal of remote sensing*, *35*(20), 7099-7117.

Goulden, T., Jamieson, R., Hopkinson, C., Sterling, S., Sinclair, A., & Hebb, D. (2014). Sensitivity of hydrological outputs from SWAT to DEM spatial resolution. *Photogrammetric Engineering & Remote Sensing*, *80*(7), 639-652.

Hodgson, M. E., & Bresnahan, P. (2004). Accuracy of airborne lidar-derived elevation. *Photogrammetric Engineering & Remote Sensing*, *70*(3), 331-339.

Hopkinson, C., Chasmer, L., Munro, S., & Demuth, M. N. (2010). The influence of DEM resolution on simulated solar radiation-induced glacier melt. *Hydrological Processes: An International Journal*, *24*(6), 775-788.

Hopkinson, C., Chasmer, L. E., Sass, G., Creed, I. F., Sitar, M., Kalbfleisch, W., & Treitz, P. (2005). Vegetation class dependent errors in lidar ground elevation and canopy height estimates in a boreal wetland environment. *Canadian Journal of Remote Sensing*, *31*(2), 191-206.

Heidemann, H. K. (2012). *Lidar base specification* (No. 11-B4). US Geological Survey.

Hunter, G. J., & Goodchild, M. F. (1996). Communicating uncertainty in spatial databases. *Transactions in GIS*, *1*(1), 13-24.

Kienzle, S. (2004). The effect of DEM raster resolution on first order, second order and compound terrain derivatives. *Transactions in GIS*, *8*(1), 83-111.

Kyriakidis, P. C., Shortridge, A. M., & Goodchild, M. F. (1999). Geostatistics for conflation and accuracy assessment of digital elevation models. *International Journal of Geographical Information Science*, *13*(7), 677-707.

Lloyd, C. D., & Atkinson, P. M. (2002). Deriving DSMs from LiDAR data with kriging. *International Journal of Remote Sensing*, *23*(12), 2519-2524.

Muane, D. (2007). Digital elevation model technologies and applications: the DEM users manual. ASPRS.

Moore, I. D., Turner, A. K., Wilson, J. P., Jenson, S. K., & Band, L. E. (1993). GIS and land-surface-subsurface process modeling. *Environmental modeling with GIS*, *20*, 196-230.

Paris, C., & Bruzzone, L. (2014). A three-dimensional model-based approach to the estimation of the tree top height by fusing low-density LiDAR data and very high resolution optical images. *IEEE Transactions on Geoscience and Remote Sensing*, *53*(1), 467-480

Quinn, P. F. B. J., Beven, K., Chevallier, P., & Planchon, O. (1991). The prediction of hillslope flow paths for distributed hydrological modelling using digital terrain models. *Hydrological processes*, *5*(1), 59-79.

Ritter, N., Ruth, M., Grissom, B.B., Galang, G., Haller, J., Stephenson, G., Covington, S., Nagy, T., Moyers, J., Stickley, J. and Messina, J., 2000. Geotiff format specification geotiff revision 1.0. *SPOT Image Corp*.

Reutebuch, S. E., McGaughey, R. J., Andersen, H. E., & Carson, W. W. (2003). Accuracy of a high-resolution lidar terrain model under a conifer forest canopy. *Canadian journal of remote sensing*, *29*(5), 527-535.

Schaer, P., Skaloud, J., Landtwing, S., & Legat, K. (2007). Accuracy estimation for laser point cloud including scanning geometry. In *Mobile Mapping Symposium 2007, Padova* (No. CONF).

Su, J., & Bork, E. (2006). Influence of vegetation, slope, and lidar sampling angle on DEM accuracy. *Photogrammetric Engineering & Remote Sensing*, *72*(11), 1265-1274.

Thieken, A. H., Lücke, A., Diekkrüger, B., & Richter, O. (1999). Scaling input data by GIS for hydrological modelling. *Hydrological processes*, *13*(4), 611-630.

Ussyshkin, R. V., & Smith, B. (2006). Performance analysis of ALTM 3100EA: Instrument specifications and accuracy of lidar data. In *ISPRS Commission I Symposium, Paris; Proceedings, part B*.

Wechsler, S. P. (2007). Uncertainties associated with digital elevation models for hydrologic applications: a review. *Hydrology and Earth System Sciences*, *11*(4), 1481-1500.

Zhang, W., & Montgomery, D. R. (1994). Digital elevation model grid size, landscape representation, and hydrologic simulations. *Water resources research*, *30*(4), 1019-1028.